

# Rotational effects on the dissociation dynamics of CHD<sub>3</sub> on Pt(111)

Gernot Füchsel,<sup>1</sup> Phillip S. Thomas,<sup>2</sup> Jurriaan den Uyl,<sup>1</sup> Yesim Öztürk,<sup>1</sup>

Francesco Nattino,<sup>1</sup> Hans-Dieter Meyer,<sup>3</sup> and Geert-Jan Kroes<sup>1</sup>

<sup>1</sup>*Leiden Institute of Chemistry, Gorlaeus Laboratories,  
Leiden University, P.O. Box 9502, 2300 RA Leiden, The Netherlands*

<sup>2</sup>*Chemistry Department, Queen's University,  
Kingston, K7L 3N6 Ontario, Canada*

<sup>3</sup>*Physikalisch-Chemisches Institut, Universität Heidelberg,  
Im Neuenheimer Feld 229, D-69120 Heidelberg, Germany*

(Dated: February 4, 2016)

## Abstract

Dissociation of methane on metal surfaces is of high practical and fundamental interest. Therefore there is currently a big push aimed at determining the simplest dynamical model that allows the reaction dynamics to be described with quantitative accuracy using quantum dynamics. Using five-dimensional quantum dynamical and full-dimensional *ab initio* molecular dynamics calculations, we show that the CD<sub>3</sub> umbrella axis of CHD<sub>3</sub> must reorient before the molecule reaches the barrier for C-H cleavage to occur in reaction on Pt(111). This rules out the application of the rotationally sudden approximation, as explicitly shown through a comparison with calculations using this approximation. Further, we suggest that the observed umbrella swing should strongly affect the sensitivity of C-H cleavage to the initial alignment of the molecule relative to the surface as found experimentally for closely related systems. We find very large differences in reactivity for molecules pre-excited to different rotational states, particularly if these states are associated with different orientations of the C-H bond.

## I. INTRODUCTION

The reactive scattering of methane from metal surfaces is an important example of a gas-surface reaction involving a polyatomic molecule. Breaking the C-H bond of CH<sub>4</sub> is a rate-limiting step in the steam reforming process [1]. Due to its technical relevance it does not come as a surprise that the system has been the subject of many experimental and theoretical investigations aimed at understanding the involved fundamental mechanisms. The dissociation of the C-H bond is nowadays considered as a prototype reaction for which the effect of vibrational excitation on the activation of a gas-surface process is extensively explored [2–6].

It has been shown that the vibrational excitation of CH<sub>4</sub> to the  $\nu_3 = 1$  state promotes the dissociation reaction on Ni(111) more than translational excitation [7]. State-resolved measurements reveal mode-specificity as pre-excitation of specific vibrational modes is more efficient at enhancing the reactivity than pre-excitation of others with similar amounts of energy added to the molecule [2, 4, 8]. Scattering experiments on vibrationally pre-excited partially deuterated methane species show bond-selectivity, *i.e.*, the possibility to break C-H bonds selectively [9, 10]. In particular for  $\nu_1$ -excited CHD<sub>3</sub>, C-H cleavage has been found to be almost 100% selective [9, 11]. But not only the initial vibrational state affects the reactivity. Experiments on CHD<sub>3</sub> reacting on Ni(100) record a significant dependence of the reaction probability on the initial alignment of the molecule with respect to the surface [12]. These features highlight the non-statistical nature of the reaction dynamics and the absence of strong surface-induced internal vibrational energy redistribution (IVR) [13].

Theory can be of great assistance by providing information about the topology of potential energy surfaces (PES) and transition state geometries, and is also able to compute the corresponding dynamics resolved in time. Much effort has been made to incorporate as many dynamical degrees of freedom (DOF) as possible in quantum mechanical simulations [14–19]. However, at present, a full-dimensional quantum dynamical description including all 15 DOF of the methane molecule is not possible with the currently available methodologies and computers. This challenges theory to develop new techniques in high-dimensional quantum dynamics (QD) as well as to determine dynamical approximations that accurately capture the physics behind the reaction.

The rotational degrees of freedom are interesting candidates to test dynamical approximations as the corresponding full basis representation of a rigid methane body scales roughly as  $\sim J_{max}^3$ , where  $J_{max}$  is the maximum total rotational angular momentum quantum number needed in the scattering basis set. There are two limits that allow for a rigorous treatment of rotation and which deserve a discussion about their applicability to molecule-surface systems involving polyatomic molecules. These are the *rotationally sudden approximation* (RSA) [20] and the *rotationally adiabatic approximation* (RAA) [21]. The former one works well when the molecule has essentially no time to rotate within the collision timescale (which is in the order of a few 100’s of femtoseconds [13]) while reacting. Some of us have recently concluded from an *ab initio* molecular dynamics (AIMD) study for the reactive scattering of CHD<sub>3</sub> from Pt(111) that such an approximation could perform well [11]. But also for atom-molecule collisions in gas phase, perspectives of the RSA model have been recently discussed in ref. [22] in the context of the sudden vector projection method [23]. In the RAA limit a process is assumed in which the molecule inherently readjusts its orientation on the

collision timescale while remaining in its initial adiabatic ground rotational or librational state, thus obeying zero-point energy conservation. Such an idea has been exploited recently for methane/surface systems in the reaction path Hamiltonian formulation [18, 19]; however, this was done in a coordinate system of normal mode vectors and not in a coordinate system including Euler angles.

In the following, we investigate the quality of these approximations for computing sticking probabilities for the reaction



on Pt(111), by comparing quantum dynamical results using different dynamical models with results of simulations that treat rotation fully, for molecules initially in the rotational ground state. For this purpose, we employ a five-dimensional (5D) quantum model including the C-H distance  $r$ , the molecule-surface distance  $Z$  and the three Euler angles  $\alpha, \beta, \gamma$ . In our model, we also allow for an adiabatic relaxation of the DCH bend angle  $\chi$ , as discussed below.

We further reinvestigate results of full-dimensional AIMD simulations in the context of the use of the rotationally sudden approximation. Based on our 5D quantum model, we also perform wave packet simulations for molecules in different initial ro-vibrational states, and discuss the importance of orientational and alignment effects on the efficiency of C-H cleavage.

The paper is organized as follows. In section II, models, the different approximations and

the methodology are explained. In section III A, results of using different rotational approximations are compared with results from simulations explicitly taking rotation into account. From there, we proceed to show in sec. III B that a reorientation of the umbrella axis of the methyl fragment is involved in the reaction and discuss in III C its potential importance for the experimentally observed rotational alignment effects for closely related systems. Section IV concludes and summarizes this work.

## II. METHODS AND MODELS

### A. Coordinates and Quantum Dynamics

We restrict ourselves to  $\text{CHD}_3$  reacting on  $\text{Pt}(111)$ , since the separation of the H-atom and the D-atom motion facilitates preselecting the most relevant dynamical coordinates for this system. We treat  $\text{CHD}_3$  as a pseudo-diatomic molecule with the  $\text{CD}_3$  umbrella fixed at its classical gas phase geometry, since for  $\nu_1$ -excited molecules and low collision energies [11, 24, 25] only C-H cleavage is observed, whereas the  $\text{CD}_3$  moiety experiences only little change at the transition state (TS) geometry. We further fix the center of mass (COM) at the top site position of the surface as it is known to be the most favorable impact site for reaction [11, 26]. The minimal model that can now be employed includes the C-H distance  $r$ , the distance of the COM of the molecule to the surface  $Z$ , and the three Euler angles. These are  $\alpha \in [0, 2\pi]$ , the azimuthal angle describing the active rotation around the space-fixed  $Z$ -axis,  $\beta \in [0, \pi]$ , the polar angle between the space-fixed  $Z$ -axis and the figure axis of  $\text{CD}_3$  (which is in our model equivalent to the  $\beta'$  angle between the principal axis of  $\text{CHD}_3$  and the surface normal), and  $\gamma \in [0, 2\pi]$ , the angle describing the rotation around the figure axis, see fig 1. Additionally, we allow for an adiabatic relaxation of the DCH bend angle  $\chi$ ,

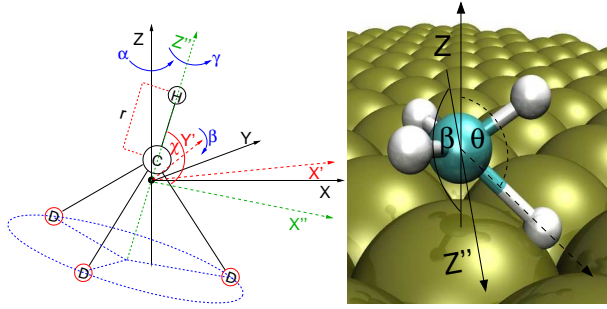


FIG. 1. Left: Dynamical coordinates used for quantum simulations including the C-H distance  $r$ , the distance of the COM of the molecule to the surface  $Z$  and the three Euler angles  $\alpha$ ,  $\beta$ ,  $\gamma$ . The DCH bend angle  $\chi$  is taken approximately into account. The Eulerian rotation matrix follows the  $ZYZ$ -convention and transforms counterclockwise. Right: A TS geometry with angle  $\theta$  between the C-H bond and the surface normal, and the angle  $\beta_{TS} = 170.5^\circ$  between the umbrella axis of the molecule and the surface normal. For the same geometry the principal axis of the molecule assumes an angle of  $\beta'_{TS} = 167^\circ$  with the surface normal.

as described below in detail.

We solve the time-dependent Schrödinger equation by using the Heidelberg Multi-Configuration Time-Dependent Hartree (MCTDH) package [27–31]. Our system Hamiltonian reads

$$\hat{H} = -\frac{\hbar^2}{2\mu} \frac{\partial^2}{\partial r^2} - \frac{\hbar^2}{2M} \frac{\partial^2}{\partial Z^2} + \frac{\hat{j}^2}{2I_B(r)} - \left( \frac{\hbar^2}{2I_C} - \frac{\hbar^2}{2I_B(r)} \right) \frac{\partial^2}{\partial \gamma^2} + V(r, Z, \alpha, \beta, \gamma; \chi), \quad (2)$$

where  $\mu$  and  $M$  are the reduced and the total mass of the molecule.  $\text{CHD}_3$  is an oblate type *symmetric top* molecule [32] with two moments of inertia  $I_A = I_B$  associated with the rotation around the molecule fixed  $X'', Y''$ -axes, and a third one,  $I_C > I_B$ , associated with the rotation around the molecule fixed  $Z''$ -axis. In our model, they have the following form

$$I_C = 3m_D r_{CD}^2 \sin^2(\chi_{eq}) \quad (3)$$

$$I_A(r) = I_B(r) = A_1 + A_2 r + A_3 r^2, \quad (4)$$

with

$$A_1 = 3m_D r_{CD}^2 \left( \frac{(m_C + m_H)}{M} \cos^2(\chi_{eq}) + \frac{1}{2} \sin^2(\chi_{eq}) \right), \quad (5)$$

$$A_2 = -\frac{6m_D m_H r_{CD} \cos(\chi_{eq})}{M}, \quad (6)$$

$$A_3 = \frac{m_H(m_C + 3m_D)}{M}. \quad (7)$$

Here,  $m_C, m_H, m_D$  are the masses of the carbon, deuterium and hydrogen atom,  $\chi_{eq} = 109.47^\circ$  is the equilibrium DCH bend angle in gas phase, and  $r_{CD} = 2.07a_0$  is the equilibrium C-D bond length.

The eigenfunctions of the  $\hat{j}^2$ -operator given in eq.(2) are the Wigner- $D$ -functions  $D_{KM}^J(\alpha, \beta, \gamma)$ , which we call  $|JKM\rangle$  in the following. Here,  $J$  is the total rotational angular momentum quantum number of  $\text{CHD}_3$ ,  $M$  is the projection of  $J$  onto the surface normal associated with the azimuthal rotation along  $\alpha$ , and  $K$  is the projection of  $J$  onto the figure axis associated with the  $\gamma$ -rotation. To make the present study possible, we implemented the Wigner- $D$ -functions and the  $\hat{j}^2$ -operator in the MCTDH package. We note that the rotational Hamiltonian given in eq. (2) is valid for  $\text{CHD}_3$  in the gas phase, and becomes inexact when molecular distortions in the bend angle break the symmetry. An exact formalism has been used in Ref. [14] to describe a similar system, but requires the inclusion of three more degrees of freedom. Our treatment, however, is in line with the approximation that the bend angle relaxation is taken into account only in the PES, as explained below. According to eq. (2) the rotational energy is given by

$$E_{J,K}^{rot} = AJ(J+1) + (C-A)K^2. \quad (8)$$

We have determined the rotational constants using our PES, and they are  $A = 3.234 \text{ cm}^{-1}$  and  $C = 2.617 \text{ cm}^{-1}$ , as found from the ro-vibrational eigenstates obtained for a molecule in the gas phase and in the vibrational ground state ( $v = 0$ ). The experimental values are  $A = 3.279 \text{ cm}^{-1}$  and  $C = 2.629 \text{ cm}^{-1}$  [32]. The quantum needed for a transition from  $v = 0$  to  $\nu_1 = 1$  and  $J = 0$  corresponds to  $2915 \text{ cm}^{-1}$  in our model and is very close to the experimental value of  $2992 \text{ cm}^{-1}$  [32]. It should be reasonable to approximate the  $\nu_1 = 1$  state as a CH-stretch state, as nine-dimensional calculations have shown that this state possesses 95% CH-stretch character [33].

Within the MCTDH approach, the wave function of the system is expanded in terms of time-dependent basis functions, *i.e.*, the so-called single-particle functions (SPFs)  $\Phi$ , and time-dependent expansion coefficients. For the present 5D system, the MCTDH wave function can then be written as

$$\Psi(r, Z, \alpha, \beta, \gamma, t) = \sum_{i_1}^{N'_r} \sum_{i_2}^{N'_Z} \sum_{i_3}^{N'_Q} A_{i_1, i_2, i_3}(t) \times \Phi_{i_1}(r, t) \Phi_{i_2}(Z, t) \Phi_{i_3}(\underline{Q}, t). \quad (9)$$

Here,  $\underline{Q} = (\alpha, \beta, \gamma)$  is a multidimensional mode combining the three Euler angles, and  $N'_r$ ,  $N'_Z$ ,  $N'_Q$  give the number of SPFs used in the dynamics for each (combined) mode. The single-particle functions themselves, however, are linear combinations of time-independent primitive basis functions. In this work, these are sinc-discrete variable representations (DVR) for the  $r$  and  $Z$  coordinate and Wigner- $D$ -functions for the Euler angles. We point out that the angles  $\alpha$  and  $\beta$  span a spherical coordinate system [34]. The Wigner- $D$ -functions can therefore be evaluated in the basis of spherical harmonics [35] by using an algorithm

Quantity	Value	Unit
MCTDH setup 5D simulations		
$N'_r$ number of SPFs* in $r$	17	
$N'_Z$ number of SPFs* in $Z$	37	
$N'_Q$ number of SPFs* in $Q = (\alpha, \beta, \gamma)$	55	
$t_f$ propagation time	500 - 800	fs
$\Delta$ error criterium for CMF-propagator[29]	1e-09	
$N_i$ maximum number of Arnoldi iterations	15	
Primitive DVR		
$r$ grid range	1.4 - 7.16	$a_0$
$Z$ grid range	3.0 - 15.8	$a_0$
$\beta$ grid range	0 - $\pi$	rad
$\alpha$ grid range	0 - $2\pi$	rad
$\gamma$ grid range	0 - $2\pi$	rad
$N_r$ number of grid points in $r$	128	
$N_Z$ number of grid points in $Z$	380	
$N_\beta$ number of grid points in $\beta$	38	
$N_\alpha$ number of grid points in $\alpha$	25	
$N_\gamma$ number of grid points in $\gamma$	25	
Complex absorbing potential		
$r_{\text{CAP}}$ start value at $r$	3.66	$a_0$
$\eta_r$ strength along $r$	0.002	$E_h$
$n_r$ order of the CAP in $r$	3	
Time CAP in $r$	100	fs
$Z_{\text{CAP}}$ start value at $Z$	13.5	$a_0$
$\eta_Z$ strength along $Z$	0.011	$E_h$
$n_Z$ order of CAP in $Z$	2	
Time CAP in $Z$	$\geq 100$	fs
Natural potential fit		
$V_{max}$ upper cut-off for potential	4.0	eV
$V_{min}$ lower cut-off for potential	-0.2	eV
Number of NPs in $r$	15	
Number of NPs in $Z$	25	
Number of NPs in $\beta$	13	
Number of NPs for combined $\alpha, \gamma$ mode	contracted	
Maximum error on all grid points	$< 1$	meV
Initial coarse grid for natural potential fit		
Number of grid points in $r$	37	
Number of grid points in $Z$	49	
Number of grid points in $\beta$	13	
Number of grid points in $\alpha$	25	
Number of grid points in $\gamma$	25	

TABLE I. Parameters used for MCTDH calculations and number of natural potentials and the initial coarse grid used in the fitting routine *potfit*. Remark\*: The number of SPFs varies for different simulations. We consider a calculation to be converged, if the population of the lowest SPF is less than 5e-05. Note, the grid range of the coarse and the primitive grid is the same. All wave packets are initially centered on  $Z_0 = 13.5 a_0$ , where the potential shows no dependence on  $Z$ .

presented in ref. [36]. Consequently, we use an exponential DVR (Fourier grid) along  $\alpha$  and  $\gamma$ , and a Gauss-Legendre DVR along  $\beta$ . In table I the most important parameters for the

converged MCTDH setup are listed.

Our simulations are carried out for translational energies  $E_{trans}$  ranging from 0.49 to up to 1.63 eV for molecules in the vibrational ground state  $v = 0$ , and  $E_{trans} \in [0.24, 0.5]$  eV for molecules in the first excited  $\nu_1 = 1$  vibrational state. In the former case, we perform three different wave packet simulations. Reaction probabilities are obtained by analyzing the flux of the wave packet fraction through the surface positioned at  $r_{CAP} = 3.66a_0$  at which an imaginary potential, called complex absorbing potential (CAP) [37, 38], here chosen to be of monomial form

$$V_{CAP} = -i\eta(q - q_{CAP})^n, \quad (10)$$

absorbs the reacting part of the wave packet, if  $q \geq q_{CAP}$ . The quantities  $n$  and  $\eta$  are the order and the strength of the CAP along the coordinate  $q$  (which is equal to  $r$  in the reactive flux analysis), respectively, and  $q_{CAP}$  marks the starting point of  $V_{CAP}$ . With the aid of the CAP we also analyzed [29, 39] the scattered wave fraction at large molecule surface distances  $Z$  (setting  $q = Z$ ). We checked that our MCTDH setup ensures that the reactive and the scattered flux sum up to about one (to within 0.006), which indicates convergence for the propagator setup and the number of SPFs used.

## B. Potential Energy Surface

The quantum dynamical (QD) simulations are performed on a reactive force field (RFF) PES that has been generated for the CH<sub>4</sub> on Pt(111) system and fitted to thousands of periodic density functional theory (DFT) points [25] to incorporate all 15 molecular degrees of freedom. In addition to the five DOFs we selected for the present dynamics study, we

also account for a change of the DCH bend angle  $\chi$  in an approximate fashion. Since the C-H bond is not aligned with the principal axis of the molecule at the TS geometry [26, 40] (see figure 1), we mimic an adiabatically relaxed dynamics by using a PES for which the molecule instantaneously assumes its most favorite configuration in  $\chi$ . There are three different DCH planes in the molecule associated with three different angles  $\chi_k$  ( $k = 1,2,3$ ). The PES is generated by selecting the optimal configuration in  $\chi_k$  for which the lowest potential energy is obtained. For this, we applied a one-dimensional search algorithm in each of the three planes, one after another, in which we allowed  $\chi_k$  to change in the selected plane while leaving the other two  $\chi_{k'}$  values intact at the tetrahedral value ( $109.47^\circ$ ). We then selected the plane and the corresponding  $\chi_k$  angle yielding the lowest potential energy. The resulting PES showed some discontinuities as we partially exceed the scope of validity of the RFF PES within the minimization procedure. We identified about 100 relevant PES points where this problem occurred and replaced the problematic values by PES values obtained from a linear interpolation of two neighboring PES points. The resulting PES is smooth and continuous.

In order to make the MCTDH method work efficiently, the PES needs to be represented in a sum of products form of so-called *natural potentials* (NPs). The Heidelberg package provides a program called *potfit*, which allows for such a transformation. However, it is not recommendable to fit the PES directly on its dynamical, also called primitive grid, as this quickly becomes unfeasible for high-dimensional systems. The recently developed multi-grid potfit (MGPF) algorithm [41] is able to generate a sum of products form of the PES in potfit-format (so called Tucker format) in a numerically more efficient way, but the MGPF code was not yet available. A way out is to first fit a coarse representation of the PES

accurately, and then to refine to the dynamical grid by using the program *chnpot*. However, this procedure needs convergence tests as different coarse grids can result in different fits. We therefore performed dynamics for fits obtained from different coarse grids that have been generated for spacings  $\Delta\beta = \pi/(N - 1)$  where  $N$  is 13 and 17. In both cases, very similar reaction probability curves were obtained from wave packet dynamics in a wide range of translational energies. In order to keep the number of expansion coefficients in the fit as low as possible, we chose to perform all following quantum simulations on a fit created for  $N = 13$ . Other parameters used for the sum of products representation are listed in table I.

### C. Dynamical approximations

When applying approximations to the rotations, the full 5D problem (eq. (2)) can be effectively reduced to two-dimensional (2D) problems. In the case of the RSA limit, the system does not reorient and dynamics is performed on individual 2D PESs along  $r$  and  $Z$  for discrete angular orientations  $(\alpha_i, \beta_j, \gamma_k)$ . For the present work, we perform  $N_\beta/2 \times N_\gamma \times N_\alpha = 11875$  single 2D simulations along  $r$  and  $Z$  as we consider values  $\beta > 90^\circ$  only, that is, orientations at which the molecule has a chance to react (see fig. 1). For  $\beta \leq 90^\circ$ , we inherently assume reaction probabilities  $P_{ijk}(E_{trans}) = 0$  for the range of translational energies  $E_{trans}$  of interest. The total reaction probability  $\overline{P}$  is obtained by the sum of all individual 2D outcomes  $P_{ijk}$  weighted according to the probability distribution of the initial rotational wave function:

$$\overline{P} = \langle JKM | P(\alpha, \beta, \gamma) | JKM \rangle \quad (11)$$

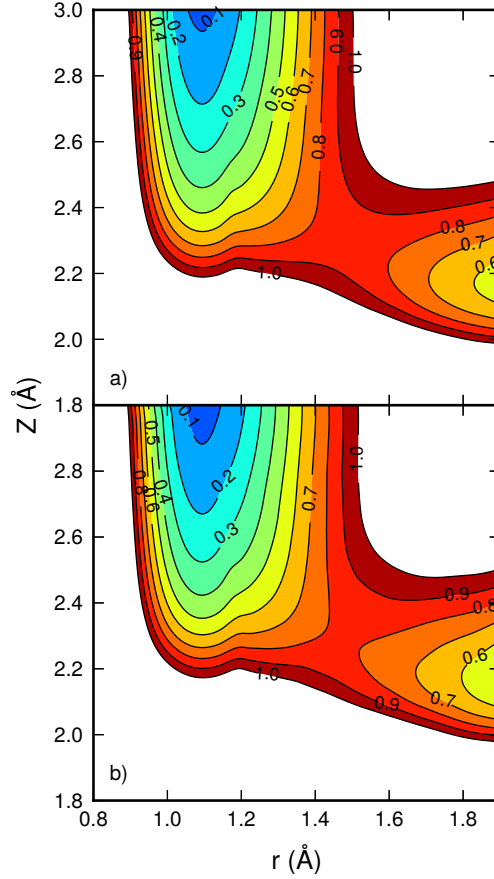


FIG. 2. Contour plots of the potential energy surfaces used for a) the rotationally adiabatic and b) the minimum pathway dynamics. Contour levels are in steps of 0.1 eV.

For the case under consideration, *i.e.*,  $|JKM\rangle = |0, 0, 0\rangle$ , eq.(11) can be numerically integrated according to

$$\bar{P}(E_{trans}) \approx \frac{\sum_{i=1}^{N_\alpha} \sum_{j=1}^{N_\beta} \sum_{k=1}^{N_\gamma} w_j P_{ijk}(E_{trans})}{N_\alpha N_\gamma \sum_{j=1}^{N_\beta} w_j}, \quad (12)$$

where  $w_j$  are the Gauss-Legendre weights.

In case of the RAA limit, the system remains in its initial rotational ground state and dynamics proceeds on an effective 2D PES along  $r$  and  $Z$  including the vibrational zero point energy (ZPE) the molecule builds up when approaching the surface. The values of this

effective PES are the lowest-lying eigenvalues obtained from a diagonalization of the rotational part of the Hamiltonian for each  $(r_i, Z_j)$ -combination. The diagonalization has been performed using the same dynamical grid point representation of the PES as used in the 5D quantum simulations. Closely related to the RAA is the minimum pathway approximation (MPA). Rotation is completely neglected and the dynamics is determined by the 2D PES  $(r, Z)$  formed from the angular orientations associated with the lowest potential energy, for each  $(r_i, Z_j)$ -combination. The adiabatic and the minimum potential energy surfaces are plotted in fig.2. Both have a typical elbow form, but they are different in the barrier height. The minimum PES has a barrier of  $E^\ddagger = 813$  meV whereas for the adiabatic one, we find  $E^\ddagger = 853$  meV. The higher barrier reflects the presence of zero point energy resulting from the rotational DOFs.

Another interesting approach is the azimuthally flat potential (AFP) approximation, which has been recently used to describe the reactive scattering of  $\text{CH}_4$  from Ni(111) [14, 16]. It is expected to work well, if the PES shows little dependence on  $\alpha$  on the way to and near the barrier. Previous electronic structure calculations suggest that this approximation is applicable to our system [26, 42], at least for low energies where reaction occurs near the top site. The AFP yields the exact quantum result for a PES with no dependence on  $\alpha$ , for which case  $M$  is a conserved quantum number. Here, we consider the case  $M = 0$  and, consequently, the number of dynamical degrees of freedom can be reduced from five to four in our model. At this point we note that all calculations with dynamical approximations are based on the dynamical grid representation of the 5D PES to ensure comparability.

### III. RESULTS

#### A. Performance of dynamical approximations

In fig.3, probability curves for the reaction given by eq. (1) obtained from different quantum simulations are shown as a function of the collision energy for molecules in a) the vibrational ground and b) the first excited vibrational state ( $v = 0, 1$ ). Since we consider only C-H bond cleavage, the reaction probability curves obtained from the RAA and the MPA calculations need to be multiplied by a factor  $1/4$ . (In the RAA and the MPA the information about the orientation of the C-H bond gets lost, so that in the same sense all orientations become equally reactive. Omitting this multiplicative factor would be tantamount to assuming that orientations, in which the D-atom points down to the surface, also lead to C-H cleavage, instead of C-D cleavage.) The figure shows that neither approach reproduces the results of the 5D dynamics, showing that these approximations are inadequate. The inadequacy of the RAA for  $\text{CHD}_3 + \text{Pt}(111)$  has been suggested and explained earlier in ref. [11]. Due to the somewhat different barriers, reaction probability curves obtained with the RAA and the MPA are slightly shifted relative to each other in the  $v = 0$  simulations. For  $v = 1$  the two curves do not reach the same reaction probability limit, which reveals the sensitivity of the dynamics to the topology of the PES even when differences are small.

With the RSA acceptable performance is not yet achieved, either, as the comparison with the 5D simulations shows, although its applicability has been previously suggested in ref.[11]. Only at low translational energies and for  $v = 1$  we find the 5D and the RSA to match well. This comes as a surprise and is probably a coincidence since the RSA is expected to work well at high translational energies, that is, on short collision timescales, on which the

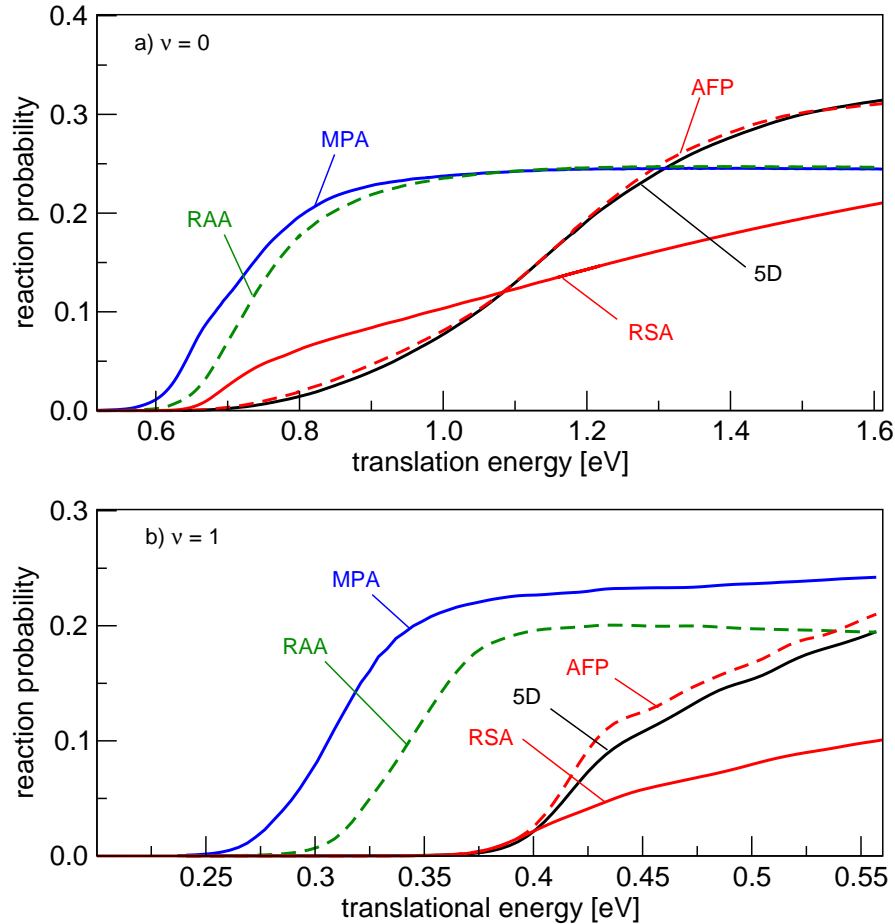


FIG. 3. Reaction probabilities as function of translational energy obtained from QD simulations for a)  $v = 0$  and b)  $v = 1$ . Shown are results taken from i) rotationally adiabatic (RAA, green dashed line), ii) minimum pathway (MPA, blue solid line), iii) rotationally sudden (RSA, red solid line), iv) azimuthally flat potential approximation (AFP, red dashed line), and v) 5D simulations (black solid line). Results for RAA and MPA are multiplied by a factor  $1/4$  to account for C-H cleavage only.

molecule does not have time to reorient while approaching the surface, and the collision time (energy) is shorter (higher) for  $v = 0$  than for  $v = 1$ .

In addition to the approximations considered above, we also tested the performance of the azimuthally flat potential (AFP) approximation, which has recently been used in ref. [14] and tested in ref. [16] for  $\text{CH}_4$  scattering on Ni(111). As explained above, this approximation allows one to reduce the number of dynamical degrees of freedom from five to four in our

model. In this work, we fix the azimuthal angle at  $\alpha = 0^\circ$  for which we find the lowest barrier height. The agreement with 5D simulations is good for  $v = 1$  but superior for  $v = 0$ . This allows us to conclude that the variation of reaction barriers along  $\alpha$  is small enough to be of little relevance for the evolution of the dynamics for molecules in their rotational ground state. We analysed the dependence of the PES on  $\alpha$  on the coarse grid representation of the PES at  $\beta = 165^\circ$ , close to the expected TS geometry. Indeed, at  $\gamma = 0^\circ$  the potential  $\overline{E}^\ddagger(\alpha) = 0.820 \pm 7$  meV shows only small variations along  $\alpha$ . For  $\alpha = 0^\circ$ , however, the variation of the potential along  $\gamma$  is slightly larger with  $\overline{E}^\ddagger(\gamma) = 0.833 \pm 13$  meV. On the other hand, as we will show below, our results indicate that a reorientation of the molecule along  $\beta$  is crucial for dissociation.

## B. Role of umbrella reorientation

In order to understand how the molecule reorients as it approaches the barrier, we now take a closer look into results obtained from full-dimensional *ab initio* molecular dynamics (AIMD) simulations recently published in ref. [11]. We consider molecules in either the vibrationally excited state ( $v = 1$ ) or in a supersonic beam, with a vibrational energy distribution characterized by the nozzle temperature  $T_n$ , denoted by "laser-off". In the latter case, we assume that the occupations of the vibrational states are given by a Boltzmann distribution of temperature  $T_n = 750$  K (for an averaged translational energy of  $\langle E_i \rangle = 0.78$  eV) and  $T_n = 850$  K (for  $\langle E_i \rangle = 0.87$  eV). More details are given in refs. [11, 43]. As mentioned above, the molecule experiences a deformation of the DCH angle  $\chi$  at the transition state, which is also reflected in our quantum model. This requires a change in  $\beta$ , the angle between the (non-reactive) umbrella axis and the surface normal, or in  $\theta$ , the

angle between the reactive bond and the surface normal, or in both. In figure 4 a-c), we plot the angular distributions of  $\beta$  and  $\theta$  of the AIMD trajectories that resulted in dissociation. We note that the AIMD trajectories for laser-off simulations describe C-H as well as C-D cleavage. The distributions are representative of the initial orientations ( $t = 0$  fs) and of the orientations, in which the reactive bond first exceeds the distance  $r = 2.83 a_0$ . Panels a) to c) show that the initial angular distributions of  $\theta$  and  $\beta$  are very similar, as would be expected for molecules in gas phase. The most favored initial orientation for reaction is located at about  $\theta = \beta \approx 124^\circ$ . At the time of reaction, the orientational distribution of the reactive bond is still close to its initial distribution, whereas the umbrella axis has reoriented to  $\beta \approx 157^\circ$ . More precisely, while the  $\theta$ -distribution does become narrower, there is no clear shift of the center of this distribution when the molecule approaches the transition state. In contrast, a clear shift occurs for the  $\beta$ -distribution. This suggests that the sudden approximation is most likely applicable to the  $\theta$  angle, but not to  $\beta$ . This is in accordance with ref. [44] where a sudden treatment of the  $\theta$  angle has brought some improvements for the calculation of sticking probabilities for  $\text{CH}_4$  on Ni(111), particularly for vibrational ground state simulations. Our findings suggest that the molecule does not react by relaxing the reactive bond along  $\theta$ , but rather by changing the orientation of the umbrella axis after passing through a *reactive gate*. This term denotes a range of  $\beta$  values through which the molecule must pass at the point where the molecule starts to interact with the surface in order to react, this range of  $\beta$  being related to, but not centered on the TS value of  $\beta$ .

From our wave packet dynamics calculations we arrive at similar conclusions. For example, the RSA reaction probability not yet integrated over  $\beta$  peaks near  $\beta \approx 157^\circ$ , see fig.4 a) to c). This value of  $\beta$  is in accordance with the AIMD results for the point at which reaction

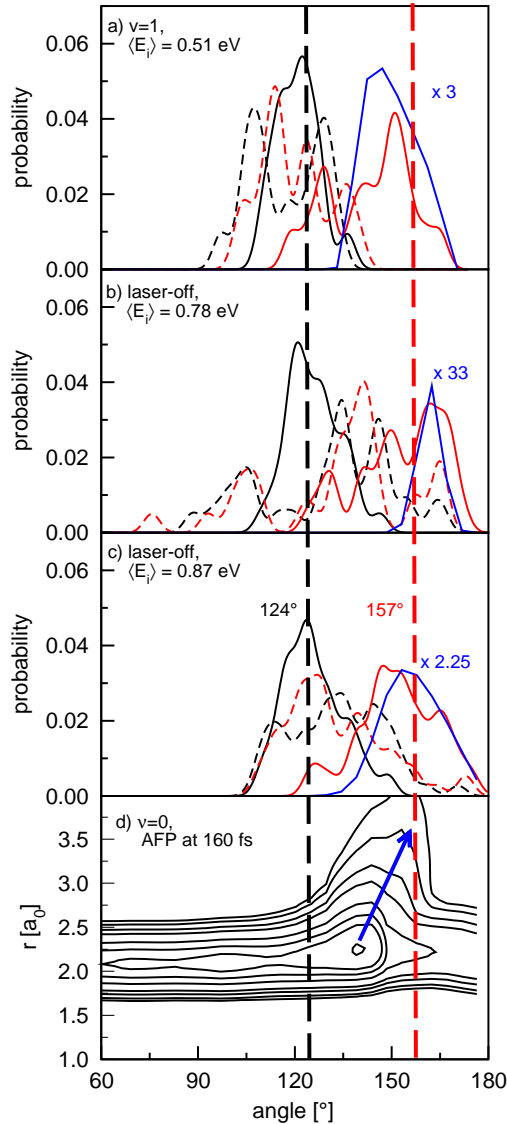


FIG. 4. Visualization of the umbrella swing for rotational ground state simulations. In panel a) to c), probability distributions of the initial ( $t = 0$  fs, dashed lines) and reactive orientation ( $r = 2.83 a_0$ , solid line) are plotted for reacting  $\text{CHD}_3$  along the angle between the surface normal and the reacting C-H bond  $\theta$  (black), and the  $\beta$  angle (red), taken from full dimensional AIMD simulations. The AIMD simulations shown in panel a) are for  $\nu_1 = 1$  excited molecules. Blue lines show the reactive  $\beta$ -distributions in RSA simulations, multiplied with different factors to put them on a comparable scale. Panel d) shows a snapshot of the wave packet density along  $r$  and  $\beta$  calculated within the AFP model at  $t = 160$  fs when reaction starts. The blue arrow indicates the wave packet motion.

occurs, and is fairly close to the  $\beta$  value near the TS. Indeed, the principal axis of the molecule at its TS geometry makes an angle of around  $\beta'_{TS} = 167^\circ$  with the surface normal,

see fig. 1. The corresponding angle between umbrella axis and surface normal is around  $\beta_{TS} = 170^\circ$ . A snapshot of the wave packet density obtained from AFP-QD simulations plotted in panel d) shows that the C-H cleavage is accompanied by a reorientation of the umbrella axis, towards  $\beta = 150^\circ$ , similar to what is observed in the AIMD from  $\beta$ . We observe that the wave packet density is concentrated near  $\beta \approx 140^\circ$  just before reaction starts. As the arrow indicates, density subsequently moves from there towards larger  $r$  values followed by a relaxation along the  $\beta$  angle, which then leads to dissociation while the remaining wave packet fraction scatters back to the gas phase. The origin of the umbrella reorientation is that it allows for a larger overlap between the  $sp^3$ -hybrid orbital at the C-atom that points towards the surface with the partly unfilled  $d$ -orbitals protruding from the metal surface.

At this point, it is useful to discuss possible scenarios describing how the molecule can assume a reactive configuration on the surface. At low collision energies, we expect the molecule to follow predominantly its dynamical minimum path along the reaction coordinate associated with the lowest barrier, and to undergo a change of the orientation of the umbrella axis (a change in  $\beta$ ). The orientations described by the reactive gate are then very important for the C-H cleavage. However, laser-off AIMD simulations at  $\langle E_i \rangle = 0.78$  eV yield an initial  $\beta/\theta$ -distribution centered on  $\beta/\theta \approx 140^\circ$  for reactive trajectories, and not on  $\beta/\theta \approx 124^\circ$  as found for the reactive AIMD trajectories calculated at slightly higher translational energies, and for the AIMD trajectories obtained for  $v = 1$  conditions. So far, we have no final explanation for this difference, but we note that laser-off simulations also include the effect of thermally excited vibrational states and it is not yet clear to us how this influences the umbrella reorientation. On the other hand, AIMD laser-off simulations at the highest collision energy of  $\langle E_i \rangle = 1.62$  eV considered (not shown in figure 4), for which the  $\beta/\theta$ -

distributions could be evaluated over 250 reactive trajectories, suggest a less pronounced effect of a reactive gate. Going to this higher  $\langle E_i \rangle$  we observe that the initial  $\beta$  distribution of the reactive trajectories broadens and that its center shifts to larger  $\beta$  values, closer to the ones of the reactive orientations. This can be interpreted as an opening of the reactive gate to a larger range of initial  $\beta$  orientations, as the increased collision energy allows the molecule to access higher barriers.

### C. Reactivity for different rotational states

We will now show that the rotational motion of the umbrella axis is most likely related to previous observations made in rotational alignment experiments for  $\nu_1 = 1$  excited  $\text{CHD}_3$  on Ni(100) [12]. There, it has been found that the reactivity is more enhanced, if the vibrational dipole moment is initially aligned parallel to the surface rather than perpendicular. The  $R(0)$  transition from the ro-vibrational ground state to the  $\nu_1 = 1$  and  $|J = 1, K = 0, M = 0\rangle$  state for the different molecular alignments is realized by adjusting the direction of the laser polarization relative to the surface normal. One can show by a coordinate transformation that the  $|1, 0, 0\rangle$  state in the laser frame corresponds to the  $|1, 0, 0\rangle$  state in the surface frame, if the laser polarization axis is perpendicularly oriented to the surface. A coherent superposition of the  $|1, 0, \pm 1\rangle$  states in the surface frame is, however, achieved, if the polarization axis is oriented parallel to the surface, see refs. [45, 46]. In the latter case the effect of the coherence on the dissociation dynamics needs to be considered as well. For the Ni(110) surface, for example, a significant dependence of the reactivity of  $\text{CH}_4$  with the azimuthal orientation of the laser polarization axis has been experimentally determined [47], thus indicating that the coherence remains when the molecule approaches the surface. The Ni(110) surface is, however, strongly corrugated, which we expect also to see in the

$\phi$ -anisotropy of the corresponding  $\text{CH}_4 + \text{Ni}(110)$  PES at the minimum barrier geometry. For the less corrugated  $\text{Ni}(100)$  surface, considered in the experiments, and the  $\text{Pt}(111)$  surface, considered here, the azimuthal dependence of the corresponding  $\text{CH}_4 + \text{surface}$  PES is small at the transition state [26], which also explains the very good performance of the AFP approximation in this work. In this case, we can assume that the coherence will have only a small or even no effect on the reactivity of the molecule, and we can simply perform the calculations for the  $M=1$  or  $M=-1$  state to compute the reactivity for the laser polarization axis lying parallel to the surface.

Under the above assumptions the experiments show that molecules with the principal axis initially aligned parallel to the surface are somewhat more reactive than molecules with the principal axis initially aligned perpendicular to the surface. This might seem to be in contradiction to the  $\beta$  orientation in the TS geometry of  $\text{CHD}_3$  on  $\text{Ni}(100)$ , which is in the range of  $160^\circ - 167^\circ$  ([42], see also below), and one therefore might expect that the perpendicular alignment favors dissociation. However, we have shown that the reaction is most likely for initial orientations with  $\beta \approx 124^\circ$ , which, as we will show below, is in qualitative agreement with the alignment contrast measured for  $\text{Ni}(100)$  being small, that is, close to zero. Since a very similar alignment dependence has been determined by experiments on  $\text{CH}_4$  scattering from a  $\text{Ni}(100)$  surface and from  $\text{Pt}(111)$  [47], it is helpful for the following discussion to assume that results for  $\text{CHD}_3$  scattering from  $\text{Ni}(100)$  are to a large extent transferable to the  $\text{Pt}(111)$  surface.

In order to reveal consequences resulting from orientational and alignment effects of the umbrella axis for dissociation, we simulate the reactivity for molecules initially in different  $J$

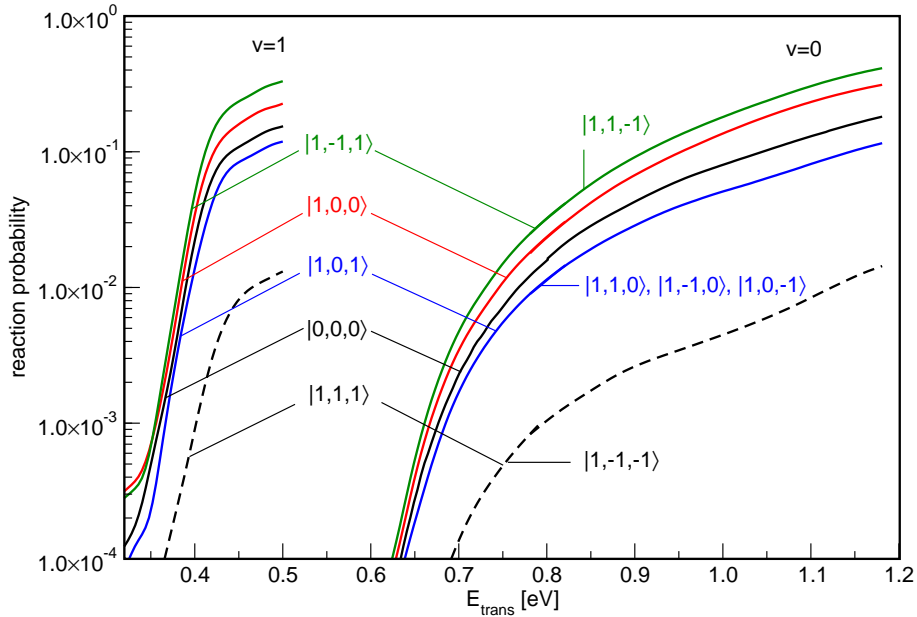


FIG. 5. Reaction probability as function of translational energy for different ro-vibrational states. The rotational states are labelled by  $|J, K, M\rangle$ .

= 1 rotational states with the help of our 5D quantum model. Reaction probability curves as functions of translational energy are plotted in figure 5 for the vibrational ground state and the first excited state. We find that the reaction probability  $P_{KM}^J(E_{trans})$  depends strongly on the initial rotational state. Reaction probability curves show the order in reactivity  $P_{-11}^1 > P_{00}^1 > P_{00}^0 > P_{01}^1 > P_{11}^1$  independent of the translational energy and the vibrational state. The following example quantifies the differences in numbers. For  $v = 0$  at  $E_{trans} = 0.8$  eV, we find that  $P_{-11}^1 : P_{00}^1 : P_{00}^0 : P_{01}^1 : P_{11}^1$  is approximately 2.0:1.5:1.0:0.7:0.07 relative to  $P_{00}^0 \approx 0.016$ . This shows that molecules in the  $|1, -1, 1\rangle$  state are about 30 times more reactive than molecules in the  $|1, 1, 1\rangle$  state. This holds true for a wide range of translational energies and is similar for molecules in the first excited vibrational state. We also note that only four curves are depicted in figure 5 although nine rotational states can be formed by different  $K, M$ -combinations and  $J = 1$ . We calculated reaction curves for all these states but find a type of pseudo-degeneracy, that is, some rotational states yield almost the same

reaction probability curves, again independent of the vibrational state.

The above observation on the one hand and the large differences in reactivity on the other hand can not be explained by differences in the rotational energy additionally put into the system, as these are only about 1 meV. Instead, orientation and alignment effects seem to be the controlling parameters for the reactivity. We therefore investigate in the following how the shape of the rotational wave function along  $\beta$  steers the efficiency of C-H cleavage. The so-called Wigner-(small) $d$ -functions  $d_{KM}^J(\beta)$  are the quantity to look at, as their square provides information about the probability  $P(\beta)$  that the umbrella axis makes an angle  $\beta$  with the space-fixed  $Z$ -axis for a particular quantum state  $|JKM\rangle$  [48]. In figure 6, we visualize

$$P(\beta) = A |d_{KM}^J(\beta)|^2 \sin(\beta) \quad (13)$$

as function of  $\beta$  for the different rotational states shown in figure 5, where  $A$  is a normalization factor. We also indicate by vertical lines the most likely initial  $\beta$  values taken from AIMD and QD simulations that lead to dissociation and, additionally, the  $\beta_{TS}$  value of the transition state geometry as shown in figure 1. We notice that molecules in rotational states that show larger overlap (*i.e.*, a higher  $P(\beta)$ ) with the reactive gate at  $\beta = 140^\circ$  have a higher chance to react. Indeed, this picture corresponds to the state-resolved dependence of the reactivity we found in figure 5. Moreover, Wigner-(small) $d$ -functions fulfill a few symmetry relations

$$\begin{aligned} d_{KM}^J(\beta) &= (-1)^{K-M} d_{MK}^J(\beta) \\ &= (-1)^{K-M} d_{-K-M}^J(\beta). \end{aligned} \quad (14)$$

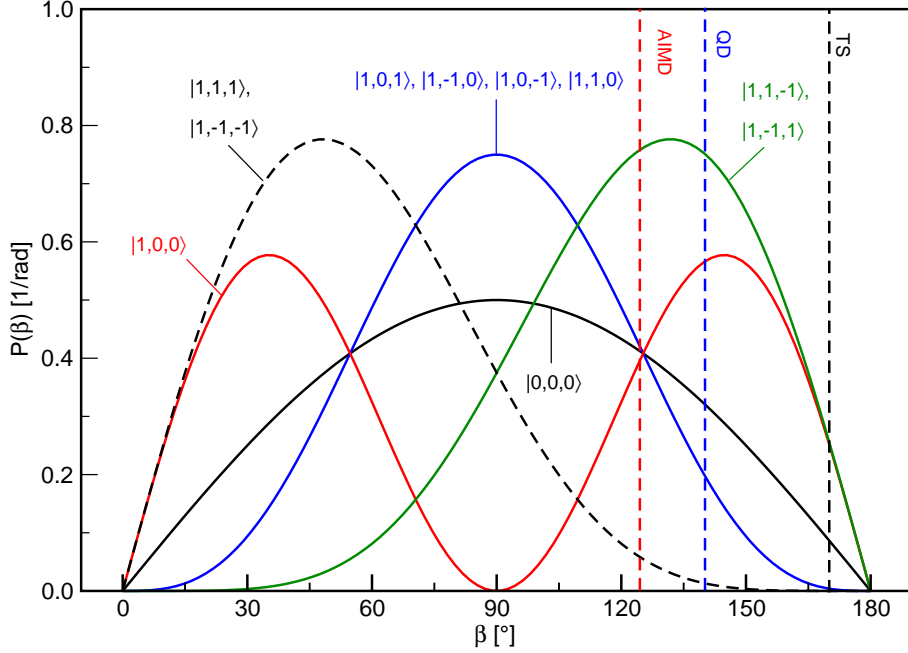


FIG. 6. Probability distribution  $P(\beta) = A|d_{KM}^J(\beta)|^2\sin(\beta)$  of finding the umbrella axis initially in a certain  $\beta$  angle according to the Wigner-(small) $d$ -functions  $d_{KM}^J(\beta)$  for different rotational states  $|J, K, M\rangle$ . The vertical dashed lines represent a) the most favored initial  $\beta$  angle for reaction in AIMD simulations (red), b) the favored  $\beta$  angle ( $140^\circ$ ) at which reaction starts in the quantum dynamics (QD, blue) and c)  $\beta_{TS} = 170^\circ$  of the transition state geometry (TS, black).

As a result, different rotational states yield the same probability distribution along  $\beta$ . The fact that the rotational states with the same  $P(\beta)$  exhibit, to within minor numerical differences, the same reaction probability curves suggest that we may refer to the reactivity of  $\text{CHD}_3$  on  $\text{Pt}(111)$  as "steric", *i.e.*, as being controlled by the molecules alignment or orientation.

When comparing with experiments on  $\text{CHD}_3$  scattering from  $\text{Ni}(100)$  and assuming that the alignment results are transferable to the  $\text{Pt}(111)$  surface, we find that our quantum results do not reproduce the enhancement of reactivity by the alignment of the molecule relative to the surface. Instead, we obtain that molecules in the state  $|1, 0, 0\rangle$ , in which the molecule is aligned perpendicular to the surface, are more reactive than molecules in the state  $|1, 0, 1\rangle$ , in

which the molecule is aligned parallel to the surface. This is in contradiction to experiments on CHD<sub>3</sub> scattering from Ni(100). For example, at  $E_{trans} = 352$  meV and  $v = 1$  a small but positive alignment contrast

$$\Delta p = \frac{P_{01}^1 - P_{00}^1}{P_{01}^1 + P_{00}^1} \quad (15)$$

of  $\Delta p = 0.178$  has been reported for CHD<sub>3</sub> on Ni(100) in ref.[12], where  $P_{01}^1$  and  $P_{00}^1$  are the sticking probabilities for molecules aligned parallel and perpendicular to the surface. As the comparison in table II shows, 5D QD simulations yield larger values with negative sign. Interestingly, AIMD simulations predict the center of the reactive gate at about  $\beta = 124^\circ$  at conditions shown in fig. 4, and no rotational alignment contrast was observed in the AIMD simulations performed for the somewhat higher  $\langle E_i \rangle$  of 0.82 eV.

	$E_i$ [meV]	$\Delta p$	$\Delta o$
Exp., Ni(100)	352	0.18	
Exp., Ni(100)	734	0.08	
5D QD, Pt(111)	352	-0.53	0.89
5D QD, Pt(111)	455	-0.32	0.93
AIMD, Pt(111)	820	0.0	

TABLE II. Alignment and orientational contrasts  $\Delta p$  and  $\Delta o$ , respectively, for  $\nu_1 = 1$  excited CHD<sub>3</sub> obtained by experiments [12, 49], 5D quantum dynamics (QD), and AIMD simulations [45] at different collision energies  $E_i$ .

The experiments on CHD<sub>3</sub> + Ni(100) and our calculations on CHD<sub>3</sub> + Pt(111) all correlate with the idea of a reactive gate in  $\beta$ , but not one that is centered on  $\beta_{TS}$ . The observations suggest a process where the molecule enters a reactive gate with a  $\beta$  value considerably lower than its  $\beta_{TS}$  value at the transition state geometry, after which the forces exerted by the surface reorient the molecule to enable reaction. This also holds true for the experiments, if one assumes that CHD<sub>3</sub> on Ni(100) and on Pt(111) are subject to the same reorientational dynamics. According to our analysis, one might expect a reactive gate centered on a  $\beta$  value

being somewhat smaller than  $120^\circ$  in order to explain experimental findings for  $\text{CHD}_3$  on Ni(100).

Our 5D quantum model does account for the reorientation effect, but it does not reproduce the location of the reactive gate obtained from AIMD simulations, and the location we suggest for the experiments on  $\text{CHD}_3$  on Ni(100). There are several reasons that can lead to these discrepancies. We start with a discussion of the discrepancies between AIMD and the QD results for  $\text{CHD}_3$  on Pt(111). The AIMD simulations were only performed for high incident energies, and they are full-dimensional including all 15 molecular DOFs and the surface motion (temperature), which was previously found to affect the efficiency of C-H cleavage in refs. [11, 15, 40, 42, 50–52]. In the current quantum simulations, however, we are considering a reduced-dimensional dynamics, and the motion along  $\chi$  is assumed to proceed adiabatically. The reorientation of the umbrella axis necessitates a relaxation along the bend angle, and we may be overestimating the ability of the molecule to relax along this coordinate in the QD calculations. Furthermore, our quantum calculations are performed for a single impact site and characteristics of the dynamics found at the top site might change at other sites. On the other hand AIMD may be incorrect at determining the reactive gate position. One possible reason for this is that there is no golden rule for forming a classical equivalent of a rotational wave function when other states than the ground state are in question. It is possible that the applied sampling procedure to create the initial conditions for trajectories (see refs. [43, 45]) influences the outcome of the simulations.

We now turn to the discrepancies between theory for  $\text{CHD}_3$  on Pt(111) and experiments for  $\text{CHD}_3$  on Ni(100). First, of course, we can not exclude the possibility that results for

Ni(100) are not transferable to the Pt(111) surface. Different surfaces might yield different alignment contrasts, with different sign. We find that the  $\beta_{TS}$  orientations in the four TS geometries published in ref. [42] for Ni(100) are between  $160^\circ$  and  $167^\circ$ , and thereby similar to, but somewhat lower than the one we obtained for the TS geometry on Pt(111) ( $\beta_{TS} = 170^\circ$ ). In addition to this, the reorientation forces on Ni(100) might be stronger than on Pt(111). However, we believe that the mechanism also underlying the rotational state dependence of the dissociation dynamics of CHD<sub>3</sub> (involving the reorientation in  $\beta$ ) is the same on both surfaces. Furthermore, for the AIMD it has also been argued that the simulations were performed at too high translational energies, that is  $\langle E_i \rangle = 0.82$  eV, for which experimental results for CHD<sub>3</sub> + Ni(100) suggest that alignment effects are less pronounced than at lower collision energies [49], see also table II. In this context, our previous discussion made in section III B appears in a new light. There, we outlined that the range of the reactive gate seems to broaden along  $\beta$  with increasing collision energy. Consequently, we expect a reduced relevance of the initial orientation of the molecule for its reactivity at higher collision energies, which would lead to smaller alignment effects, as also observed in experiments [49]. But also the underlying DFT methodology used to describe the PES can influence our results. Our study is based on the Perdew-Burke-Ernzerhof (PBE) DFT functional [53]. The use of another *generalized gradient approximation* (GGA) DFT functional and the inclusion of van der Waals (vdW) forces to account for long-range interactions have very recently been tested on the CHD<sub>3</sub> on Pt(111) system and have been shown to improve the performance of dynamical simulations in comparison to experiments [43, 45].

From looking at the probability distribution of the oriented states  $|1, 1, 1\rangle$  and  $|1, -1, 1\rangle$  in figure 6, and their analogous states,  $|1, -1, -1\rangle$  and  $|1, 1, -1\rangle$ , respectively, an accurate

description of the reactive gate position is not needed in order to predict the dependence of the reactivity on these states at least qualitatively. The reactive C-H bond of molecules in the  $|1, -1, 1\rangle$  state is pointing towards the surface, and away from the surface, if molecules are in the  $|1, 1, 1\rangle$  state. Consequently, dissociation is not efficient for the latter case, which we would expect to observe, if the analogous experiment would be performed. At  $E_{trans} = 455$  meV and  $v = 1$ , our simulations predict an orientational contrast

$$\Delta o = \frac{P_{-11}^1 - P_{11}^1}{P_{-11}^1 + P_{11}^1} \quad (16)$$

of  $\Delta o = 0.930$ , where  $P_{-11}^1$  and  $P_{11}^1$  are the sticking probabilities for molecules with a C-H bond pointing towards and away from the surface, respectively. This large orientational contrast is similar at lower collision energies, see table II, and emphasizes the importance of the initial rotational state for the reactivity at conditions that allow only for C-H cleavage.

We have also investigated the reactivity of molecules in rotational states with a total rotational angular momentum quantum number  $J = 2$ . We find qualitatively the same characteristics as above. When going to higher  $J \geq 5$  states and  $M = K = 0$ , we observed that reactivity increases with increasing  $J$ . However, at high collision energies we also find that reaction curves start crossing each other. For example, molecules in  $|5, 0, 0\rangle$  are more reactive for  $E_{trans} > 1.15$  eV than molecules in states with  $J \in [6, 10]$ . This phenomenon has been previously observed in theoretical works [54, 55] and in experiments [56] on methane scattering from Ni surfaces. It possibly indicates the presence of dynamical steering effects that make the conversion of translational energy into the motion along the reaction coordinate more efficient for low  $J$  values at a certain point.

Interestingly, a strong influence of the rotational state on the stereospecific chemistry of  $\text{CHD}_3$  has also been observed in reactive collisions with atoms in the gas phase, for example in [57–61]. The  $K, M$  quantum numbers also control the orientation of the C-H bond relative to the reaction partner in these cases, which either results in favorable or unfavorable configurations, promoting or inhibiting the reaction. Also for water reacting with the Cu(111) surface, a previous theoretical study [62] suggests a considerable influence of the initial rotational state on the dissociation dynamics of  $\text{H}_2\text{O}$ .

The success of the projection method implied by our results (in which the reactivity of molecules in  $|JKM\rangle$  states would be determined by projecting  $P_{KM}^J(\beta)$  on the reactive gate) is by no means a foregone conclusion, and the approach may not be applicable to all (partially) deuterated methane species, at least not in the same manner.  $\text{CHD}_3$  and  $\text{CH}_3\text{D}$  are *symmetric top* molecules and the alignment or orientation of the angular momentum vector  $\vec{J}$  has clear consequences for the alignment/orientation of the C-H and C-D bond, respectively. On the other hand,  $\text{CH}_4$  is a *spherical top* and  $\text{CH}_2\text{D}_2$  is an *asymmetric top* molecule. The orientation of the figure axis is in these cases not necessarily associated with the orientations of reactive bonds. A procedure in which the rotational wave function is projected on the reactive gate in order to explain the alignment effects, measured for  $\text{CH}_4$  on Ni(100), Ni(110), Ni(111), and Pt(111) [47, 49] is then no longer so straightforward.

#### IV. CONCLUSION AND OUTLOOK

In this work, we reported on the performance of different dynamical approximations to rotation to describe the reactive scattering of  $\text{CHD}_3$  on Pt(111) quantum mechanically, and

on the effect of the initial rotational state of the molecule on C-H cleavage.

The rotationally sudden and the rotationally adiabatic approximations fail to reproduce 5D simulations that fully account for rotation in the three Euler angles. The failure of the RSA indicates that reorientation effects, as found to occur in the angle  $\beta$  between the  $\text{CD}_3$  umbrella axis and the surface normal, play an important role in the dissociation dynamics. On the other hand, the RAA clearly overestimates the forces resulting from the PES that can keep the molecule in its initial rotational ground state. The azimuthally flat potential (AFP) approximation, however, shows good to very good performance, which points to a small anisotropy of the PES in  $\alpha$ . However, at present, we cannot make a definite statement whether the molecule behaves similarly at different adsorption sites than the top site. It would be interesting to validate the performance of the AFP approximation at other sites using the current model and PES, or even to account for the motion of the molecule along the surface. It was recently stated that an explicit treatment of the azimuthal rotation can become necessary at sites other than the top site for the related  $\text{CH}_4$  on Ni(111) system [16].

We find strong evidence that molecules reorient their umbrella axis on the way to the barrier. Our 5D quantum simulations as well as full-dimensional AIMD simulations are consistent with this observation. As a consequence, only those molecules proceed to the reaction barrier that pass through a reactive gate centered on  $\beta \approx 140^\circ$  in quantum simulations and on  $\beta \approx 124^\circ$  in AIMD simulations performed for higher collision energies. In both cases, this orientation differs from the orientation in the TS state geometry, in agreement with the interpretation of experimental data [12]. Indeed, our results suggest for the  $\text{CHD}_3 + \text{Ni}(100)$  system a reactive gate at  $\beta < 120^\circ$  while the corresponding four TS geometries

published in ref. [42] show that the umbrella axis assumes values between  $\beta = 160^\circ - 167^\circ$ . We further obtain that the initial rotational state of the molecule in gas phase considerably affects its activity for reaction. Molecules in differently oriented states (reactive C-H bond points down or up) show the largest differences in reactivity. The dependence of the reaction probability on the initial rotational state as well as the observed steric reactivity can be understood by looking at the overlap of the initial probability distributions  $P(\beta)$  with the position of the reactive gate in  $\beta$ . Our results suggest that the larger the overlap is, the higher the dissociation probability is likely to be.

The reorientational dynamics describes a change of  $\beta$  from the reactive gate value to the TS value. An accurate description should then require an accurate dynamical model and PES. A more sophisticated representation treating the DCH bend angle relaxation fully quantum mechanically as employed in ref. [14–16] could be tested for its performance in reproducing the rotational alignment experiments. But it is also desirable to evaluate the accuracy of different density functionals, for instance, including vdW corrections, in the description of the molecule-surface interaction. Quantum and AIMD simulations should also be performed to describe the reactive scattering of  $\text{CHD}_3$  from the Ni(100) surface to determine whether the observed discrepancies between calculations on  $\text{CHD}_3 + \text{Pt}(111)$  and experiments on  $\text{CHD}_3 + \text{Ni}(100)$  are not simply due to differences between the systems on which the calculations and the measurements were performed, such as the somewhat different  $\beta_{TS}$ , and, possibly, differences in the strength of the reorientation forces.

Of great importance, we believe, would be experiments on orientation effects for the system we considered. It would also be interesting to see, if reactive scattering experiments on

CHD<sub>3</sub> reveal similar alignment effects at the Ni(100) and at Pt(111) surface, or even at other surfaces. Experiments on different isotopomers of methane could shed light on the role played by orientation/alignment effects on their reactivity, and the mechanisms that would allow control of the reaction by exploiting the possibility of orienting/aligning molecules relative to the surface by controlling their initial rotational state population.

## V. ACKNOWLEDGEMENT

We thank Ariel Lozano and Fabio Busnengo for providing the exact fit parameters used for the RFF PES and for their assistance in programming the PES, and Bret Jackson for providing the TS geometries for CH<sub>4</sub> on Ni(100) and for useful discussions. We also thank Matteo Bonfanti for fruitful discussions and Mark Wijzenbroek for assistance with figures. Our investigations were carried out on the Dutch national e-infrastructure with the support of NWO-EW. We thank CW-NWO for supporting this research through a TOP grant and the European Research Council for funding through an ERC-2013 advanced grant (Nr. 338580).

- 
- [1] G. Jones, J. G. Jakobsen, S. S. Shim, J. Kleis, M. P. Andersson, J. Rossmeisl, F. Abild-Pedersen, T. Bligaard, S. Helveg, B. Hinnemann, J. R. Rostrup-Nielsen, I. Chorkendorff, J. Sehested and J. K. Nørskov, *J. Catal.*, 2008, **259**, 147 – 160.
- [2] R. D. Beck, P. Maroni, D. C. Papageorgopoulos, T. T. Dang, M. P. Schmid and T. R. Rizzo, *Science*, 2003, **302**, 98–100.
- [3] B. Jiang, M. Yang, D. Xie and H. Guo, *Chem. Soc. Rev.*, 2016, <http://dx.doi.org/10.1039/C5CS00360A>.

- [4] L. Juurlink, D. Killelea and A. Utz, *Prog. Surf. Sci.*, 2009, **84**, 69 – 134.
- [5] H. Chadwick and R. D. Beck, *Chem. Soc. Rev.*, 2016, <http://dx.doi.org/10.1039/C5CS00476D>.
- [6] G.-J. Kroes, *J. Phys. Chem. Lett.*, 2015, **6**, 4106–4114.
- [7] R. R. Smith, D. R. Killelea, D. F. DelSesto and A. L. Utz, *Science*, 2004, **304**, 992–995.
- [8] L. B. F. Juurlink, P. R. McCabe, R. R. Smith, C. L. DiCologero and A. L. Utz, *Phys. Rev. Lett.*, 1999, **83**, 868–871.
- [9] D. R. Killelea, V. L. Campbell, N. S. Shuman and A. L. Utz, *Science*, 2008, **319**, 790–793.
- [10] P. M. Hundt, H. Ueta, M. E. van Reijzen, B. Jiang, H. Guo and R. D. Beck, *J. Phys. Chem. A*, 2015, **119**, 12442–12448.
- [11] F. Nattino, H. Ueta, H. Chadwick, M. E. van Reijzen, R. D. Beck, B. Jackson, M. C. van Hemert and G.-J. Kroes, *J. Phys. Chem. Lett.*, 2014, **5**, 1294–1299.
- [12] B. L. Yoder, R. Bisson and R. D. Beck, *Science*, 2010, **329**, 553–556.
- [13] D. R. Killelea and A. L. Utz, *Phys. Chem. Chem. Phys.*, 2013, **15**, 20545–20554.
- [14] B. Jiang, R. Liu, J. Li, D. Xie, M. Yang and H. Guo, *Chem. Sci.*, 2013, **4**, 3249–3254.
- [15] X. Shen, Z. Zhang and D. H. Zhang, *Phys. Chem. Chem. Phys.*, 2015, **17**, 25499–25504.
- [16] X. Shen, J. Chen, Z. Zhang, K. Shao and D. H. Zhang, *J. Chem. Phys.*, 2015, **143**, 144701.
- [17] P. M. Hundt, B. Jiang, M. E. van Reijzen, H. Guo and R. D. Beck, *Science*, 2014, **344**, 504–507.
- [18] B. Jackson and S. Nave, *J. Chem. Phys.*, 2011, **135**, 114701.
- [19] M. Mastromatteo and B. Jackson, *J. Chem. Phys.*, 2013, **139**, 194701.
- [20] R. D. Levine, *Chem. Phys. Lett.*, 1969, **4**, 211 – 213.
- [21] R. D. Levine, *J. Chem. Phys.*, 1968, **49**, 51–55.
- [22] B. Jiang, J. Li and H. Guo, *J. Chem. Phys.*, 2014, **140**, 034112.

- [23] H. Guo and B. Jiang, *Acc. Chem. Res.*, 2014, **47**, 3679–3685.
- [24] L. Chen, H. Ueta, R. Bisson and R. D. Beck, *Farad. Discuss.*, 2012, **157**, 285–295.
- [25] X. J. Shen, A. Lozano, W. Dong, H. F. Busnengo and X. H. Yan, *Phys. Rev. Lett.*, 2014, **112**, 046101.
- [26] S. Nave and B. Jackson, *J. Chem. Phys.*, 2009, **130**, 054701.
- [27] G. A. Worth, M. H. Beck, A. Jäckle and H.-D. Meyer, The MCTDH Package, Version 8.2, (2000). H.-D. Meyer, Version 8.3 (2002), Version 8.4 (2007). Used version: 8.4.10 (2014). See <http://mctdh.uni-hd.de>.
- [28] H.-D. Meyer, U. Manthe and L. Cederbaum, *Chem. Phys. Lett.*, 1990, **165**, 73 – 78.
- [29] M. H. Beck, A. Jäckle, G. A. Worth and H.-D. Meyer, *Phys. Rep.*, 2000, **324**, 1–105.
- [30] H.-D. Meyer, *WIREs Comp. Mol. Sci.*, 2012, **2**, 351–374.
- [31] H.-D. Meyer, F. Gatti and G. A. Worth, *Multidimensional Quantum Dynamics: MCTDH Theory and Applications*, Wiley-VCH, Weinheim, 2009.
- [32] O. Ulenikov, E. Bekhtereva, S. Albert, S. Bauerecker, H. Hollenstein and M. Quack, *Mol. Phys.*, 2010, **108**, 1209–1240.
- [33] X.-G. Wang and E. L. Sibert III, *J. Chem. Phys.*, 1999, **111**, 4510–4522.
- [34] J. D. Pendleton, *Am. J. Phys.*, 2003, **71**, 1280–1291.
- [35] M. A. Blanco, M. Flórez and M. Bermejo, *Comp. Theor. Chem.*, 1997, **419**, 19 – 27.
- [36] H. Dachsels, *J. Chem. Phys.*, 2006, **124**, 144115.
- [37] U. V. Riss and H.-D. Meyer, *J. Phys. B*, 1993, **26**, 4503–4535.
- [38] U. V. Riss and H.-D. Meyer, *J. Chem. Phys.*, 1996, **105**, 1409–1419.
- [39] S. Sukiasyan and H.-D. Meyer, *J. Chem. Phys.*, 2002, **116**, 10641–10647.
- [40] A. Lozano, X. Shen, R. Moiraghi, W. Dong and H. Busnengo, *Surf. Sci.*, 2015, **640**, 25 – 35.

- [41] D. Peláez and H.-D. Meyer, *J. Chem. Phys.*, 2013, **138**, 014108.
- [42] S. Nave, A. K. Tiwari and B. Jackson, *J. Chem. Phys.*, 2010, **132**, 054705.
- [43] F. Nattino, *Ph.D. thesis*, Leiden University, 2015.
- [44] B. Jackson, F. Nattino and G.-J. Kroes, *J. Chem. Phys.*, 2014, **141**, 054102.
- [45] F. Nattino, D. Migliorini, M. Bonfanti and G.-J. Kroes, *J. Chem. Phys.*, 2016, **144**, 044702.
- [46] D. M. Brink and G. R. Satchler, *Angular Momentum*, Oxford University Press, 1968.
- [47] B. L. Yoder, R. Bisson, P. Morten Hundt and R. D. Beck, *J. Chem. Phys.*, 2011, **135**, 224703.
- [48] R. N. Zare, *Angular Momentum*, John Wiley & Sons, Inc., New York, 1988.
- [49] B. L. Yoder, *Steric Effects in the Chemisorption of Vibrationally Excited Methane on Nickel*, Springer, Berlin, 2012.
- [50] A. C. Luntz and D. S. Bethune, *J. Chem. Phys.*, 1989, **90**, 1274–1280.
- [51] A. K. Tiwari, S. Nave and B. Jackson, *Phys. Rev. Lett.*, 2009, **103**, 253201.
- [52] A. K. Tiwari, S. Nave and B. Jackson, *J. Chem. Phys.*, 2010, **132**, 134702.
- [53] J. P. Perdew, K. Burke and M. Ernzerhof, *Phys. Rev. Lett.*, 1996, **77**, 3865–3868.
- [54] Y. Xiang, J. Z. H. Zhang and D. Y. Wang, *J. Chem. Phys.*, 2002, **117**, 7698–7704.
- [55] M.-N. Carré and B. Jackson, *J. Chem. Phys.*, 1998, **108**, 3722–3730.
- [56] L. B. F. Juurlink, R. R. Smith and A. L. Utz, *Farad. Discuss.*, 2000, **117**, 147–160.
- [57] F. Wang, J.-S. Lin and K. Liu, *Science*, 2011, **331**, 900–903.
- [58] F. Wang, K. Liu and T. P. Rakitzis, *Nat. Chem.*, 2012, **4**, 636–641.
- [59] Z. Zhang and D. H. Zhang, *J. Chem. Phys.*, 2014, **141**, 144309.
- [60] R. Liu, F. Wang, B. Jiang, G. Czakó, M. Yang, K. Liu and H. Guo, *J. Chem. Phys.*, 2014, **141**, 074310.
- [61] G. Czakó, *J. Phys. Chem. A*, 2014, **118**, 11683–11687.

[62] B. Jiang, J. Li, D. Xie and H. Guo, *J. Chem. Phys.*, 2013, **138**, 044704.